Self-Sustained Libration Regime in Nonlinear Microelectromechanical Devices

Samer Houri ⬤,* Motoki Asano, Hajime Okamoto ⬤, and Hiroshi Yamaguchi

*NTT Basic Research Laboratories, NTT Corporation, 3-1 Morinosato-Wakamiya, Atsugi-shi, Kanagawa
243-0198, Japan*

We present a mode of operation for Duffing-type nonlinear microelectromechanical system devices whereby a self-sustained multifrequency output is generated. This self-sustained librator regime creates a limit cycle around a dynamical fixed point, i.e., around fixed points within the rotating frame, whereas a traditional oscillator generates a limit cycle around a static fixed point. The librator limit cycles thus created do not change the global topology of the rotating frame phase space, but are constrained by it. Because of the Duffing nonlinearity, different types of limit cycles could be generated within the same phase space, with each type possessing distinct dynamical features. Transitioning between these limit cycles requires crossing homoclinic bifurcations, which is done without generating chaos as the phase space dynamics are constrained in two dimensions. This work provides an alternative experimental tool for the study of microelectromechanical and nanoelectromechanical system dynamics and their application.

I. INTRODUCTION

Self-oscillating systems (or simply oscillators), defined as systems that produce a periodic output without being periodically driven [1], are omnipresent in the physical [2], biological [3,4], and engineering fields [5]. Indeed, oscillators are at the center of modern electronic instruments as they provide frequency and timing references [6]. Microelectromechanical system (MEMS) and nanoelectromechanical system (NEMS) devices in particular represent an interesting medium for the realization of self-oscillating systems as they provide high quality factors, low-power operation, and on-chip integration capabilities [7]. In dynamical terms, a self-sustained periodic motion is described as a limit cycle, defined as a closed attracting orbit in the corresponding phase space [8].

Beyond their time keeping role, oscillators are also crucial for the study of complex phenomena that arise due to their coupling, such as synchronization [9], chimeras [10], and phase patterns [11]. Furthermore, large networks of coupled oscillators form the building blocks for new computational techniques such as neuromorphic computing [12] and reservoir computation [13].

However, in physical and engineering systems limit cycles are equally encountered as an incidental instability (i.e.,, a Hopf bifurcation) that is generated by the dynamical interactions within the system. Such emerging limit cycles have been widely detected in MEMS and NEMS systems, examples of which include cases of synchronized nanomechanical oscillators [14,15], cases of internal resonance in MEMS and NEMS devices [16–21], or even strongly driven MEMS resonators [22].

The MEMS and NEMS examples stated above share the common denominator of having these incidental limit cycles taking place on top of an already existing periodically forced motion, thus changing the system dynamics from periodic to quasiperiodic. More specifically, these Hopf bifurcations take place in the slow dynamics, i.e., rotating frame, whereby the stability of the fixed point within the rotating frame, i.e., the steady-state solution, is changed and a limit cycle is created in its stead [9,14–23].

Furthermore, since these limit cycles are taking place within the slow dynamics of a MEMS or NEMS device, their frequencies are on long time scales compared to the fast forced oscillations of the system. Thus, the driven system dynamics change into a fast forced periodic motion modulated via a slow superimposed limit cycle.

Regardless of whether such unanticipated limit cycles are considered beneficial or detrimental to the functioning of MEMS and NEMS devices or their performance, they have not been satisfactorily explored, nor pursued for their own sake. In addition, since the instabilities that lead to these rotating frame limit cycles usually depend on a multitude of device and modal parameters, the limit cycle properties (e.g., amplitude and frequency) cannot be controlled, and their existence is constrained to a limited region in parameter space; see, for instance, Ref. [23]. Thus, such rotating frame limit cycles may only be generated in special devices, under particular operating conditions, and their properties are not readily controllable.

*samer.houri.dg@hco.ntt.co.jp

This work aims to explore these rotating frame limit cycles, and provide a definite means to generate them electronically in a generic single degree of freedom MEMS or NEMS resonator, and to do so in a controllable manner such that they cover larger frequency and amplitude ranges. Hence, this work provides the means for the generation of exotic and interesting dynamics as well as offers an alternative experimental tool previously unavailable to the MEMS-NEMS community.

MEMS and NEMS resonators constitute an ideal platform to further investigate such dynamics, as they offer easy experimental control, good quality factors, interesting time scales making the slow-fast time scales easy to resolve experimentally, and the presence of Duffing-type nonlinearity [24–26]. Furthermore, the dynamics of MEMS and NEMS devices can be treated using perturbation techniques such as the rotating frame approximation (RFA). The RFA permits the averaging out of fast oscillations, leaving a small envelope around a resonance mode in which the dynamics take place.

Since the RFA phase space can be manipulated by simply modifying the parameters of the externally applied driving force, fixed points can be created and manipulated without requiring device or setup redesign. This experimental flexibility explains the recent interest in the RFA dynamics of MEMS and NEMS nonlinear devices, where rotating frame dynamics have been used to demonstrate noise squeezing [27], chaos [28], as well as solitons [29] and pseudoangular momenta systems [30].

As stated, this work introduces an experimental approach for the creation and manipulation of rotating frame limit cycles; in addition, we aim to leverage the controllable RFA phase space to demonstrate a richer dynamical behavior when compared to the limit cycles in the case of conventional oscillators, i.e., limit cycles in the laboratory frame [5,31–33]. We label these rotating frame limit cycles "librators," and model and experimentally explore their behavior.

Libration is a term used in the context of Hamiltonian celestial mechanics to indicate periodic motion around a dynamical fixed point, for example when a spacecraft orbits one of the Lagrangian points in the Earth-Moon or Sun-Earth rotating frame [34–36]. And although the term libration is sometimes used to designate a different dynamical aspect [8,37–41], we employ the term in this work to only indicate periodic orbits around dynamical fixed points.

Furthermore, we extend the concept of libration orbits and use the term librator to indicate a limit cycle created around a dynamical fixed point (i.e., in the rotating frame) of a microelectromechanical system, in analogy with the use of the terms oscillation and oscillator. The distinction between librator and oscillator being that whereas the former's limit cycle is created around a dynamical fixed point, the latter's is created around a static fixed point, usually the

rest position. Therefore, the output of a librator as seen in the laboratory frame is (nearly) quasiperiodic, whereas that of an oscillator is periodic.

As will be shown below, the librator affords access to highly unusual and interesting dynamics; for instance, the creation, in a controllable manner, of a rotating frame phase space that supports distinct types of structurally stable limit cycles that are separated by homoclinic bifurcations. More importantly, since the dynamics of the librator are fully contained in a two-dimensional phase space, the crossing of the homoclinic does not result in the onset of chaos, thus enabling new exotic and chaosless dynamics. This is an experimental demonstration of a controllable homoclinic bifurcation in a microelectromechanical system, despite previous interesting indications of transient critical slowing down in ring-down measurements [42].

In the scientific literature, quasiperiodic motion in MEMS and NEMS devices has been proposed as a potential means to generate phononic frequency combs, or as a MEMS or NEMS sensor's readout mechanism [43–45]. Thus, in addition to providing an alternative experimental tool for MEMS and NEMS devices, the quasiperiodic nature of the librator dynamics can be used for similar applications to those mentioned while offering better control over the amplitude and frequency of the quasiperiodic components.

II. THEORY AND MODELING

To properly introduce the concept of librator, we start by considering a driven weakly nonlinear Duffing-type MEMS resonator, and to simplify matters further, we consider the resonator to be driven outside the hysteretic region, i.e., outside the bistable region, as shown in Fig. 1(a). Such a system will have a steady-state response, i.e., a vibration amplitude, dictated by its parameters and those of the external forcing. If the system is perturbed from its steady state, it will undergo a transient oscillation on top of the drive oscillation as it returns to its original amplitude [46,47]. Seen in the rotating-frame phase space, this transient corresponds to the system tracing a spiral as it approaches the steady-state fixed point, as shown in the inset of Fig. 1(a). The situation becomes more interesting if the libration motion is undamped; in such a case the small perturbation will persist and will continuously orbit the fixed point in the rotating frame, resulting in an undamped libration oscillation; see Fig. 1(a). This concept may be further extended by the deliberate creation of a limit cycle around the rotating-frame fixed point; in such a situation the originally attracting fixed point becomes a repeller and a stable limit cycle is created around the, now unstable, fixed point. Thus, libration oscillations are now self-sustained and the system is a librator; see Fig. 1(a).

Driving a nonlinear resonator with sinusoidal forcing results in a steady-state solution that is represented by a
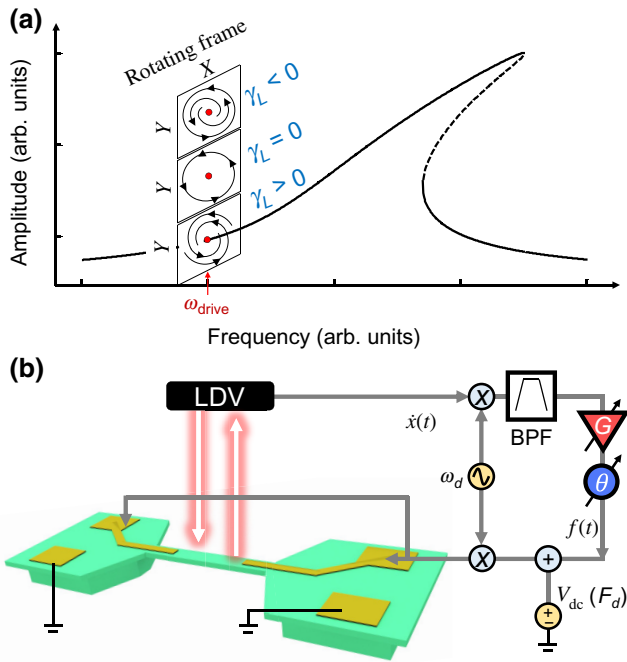
FIG. 1. (a) Schematic representation of a librator. A nonlinear resonator driven outside the bistable regime has a single steady-state solution, i.e., fixed point, in the rotating frame phase space (red dots). A perturbation around the steady-state results in a transient response in which the system slowly spirals back towards the fixed point (bottom inset). If the libration damping (γ_L) is zero, i.e., $\gamma_L = 0$, then the perturbation will persist as a periodic motion in the rotating frame phase space orbiting the fixed point (middle inset). if the libration damping is negative, i.e., $\gamma_L < 0$, the fixed point becomes unstable and leads to a limit cycle being created in the rotating frame phase space (top inset). (b) Feedback loop for the creation of a librator. The structure's motion is measured using a laser Doppler vibrometer (LDV), its output [$\dot{x}(t)$] is then down-converted, band-pass filtered (BPF), amplified (G), and phase shifted (θ), before adding a dc voltage component that corresponds to the steady-state forcing (F_d), and then up-converted to the drive frequency (ω_d) and injected to drive the MEMS device.

fixed point within the rotating frame, or two stable fixed points and one saddle point in case the system is driven into the bistable regime. Since the dynamics we seek, i.e., the limit cycle, is equally supposed to take place within the rotating frame, it is clear that simply forcing the device with a sinusoidal drive is not enough; hence, additional terms are needed to create the interesting dynamics. Therefore, the standard equation of a driven nonlinear resonator [24] is modified to include an additional term in the rotating frame, indicated by $f(t)$; the equation now reads

$$\ddot{x} + (\gamma + \beta x^2)\dot{x} + \omega_0^2 x + \alpha x^3 = [F_d + f(t)]\cos(\omega_d t),$$
(1)

where x is the displacement; γ, β, ω_0, α are respectively the linear damping, nonlinear damping, natural frequency,

and Duffing nonlinearity of the resonator; F_d and ω_d are the amplitude and frequency of the applied external forcing; and $f(t)$ is the additional term necessary to create a limit cycle within the rotating frame. Both F_d and $f(t)$ will be given in units of volts throughout this text; however, in order to balance the equation, a transduction coefficient η is implicitly included in those terms. In addition, a detuning parameter δ is introduced such that $\omega_d = \omega_0(1 + \delta)$. We also introduce the scaled constants as $\bar{t} = t\omega_0$, $\bar{\gamma} = \gamma/\omega_0$, $\bar{\alpha} = \alpha/\omega_0^2$, $\bar{\beta} = \beta/\omega_0$, $\bar{F}_d = F_d/\omega_0^2$, and $\bar{f}(t) = f(t)/\omega_0^2$. Hereon, all equations are written using this form, but the bars are dropped for convenience. Note that the terms γ, β, α, F_d, δ, and $f(t)$ are all perturbation order terms, i.e., approximately $\mathcal{O}(\epsilon)$, thus indicating a weakly nonlinear, weakly forced system.

The usual approach to creating a limit cycle in a MEMS oscillator consists of inserting a resonator in a feedback loop; as the gain of the feedback loop is increased, the effective damping of the resonator (γ_{eff}) is decreased until it becomes negative and a limit cycle is thus created [48–52]. This approach is not suitable for librators that impose two conditions. First, since the limit cycle is to be created in the rotating frame, the feedback needs to be applied only in the rotating frame; hence, the feedback term [$f(t)$] in Eq. (1) is multiplied by the driving frequency that acts as a carrier frequency. Second, since the aim is to create a limit cycle around the driven fixed point(s), the response corresponding to the driven term needs to be excluded from the feedback loop so it would not be amplified.

It is possible to think of the feedback term $f(t)$ in analogy with the feedback in a classical oscillator system [48–52]. Wherein for a classical oscillator the feedback reduces the damping (linewidth) of the device until reaching zero at the onset of self-oscillation, the term $f(t)$ reduces the damping (linewidth) of the libration motion (and only the libration motion) within the rotating frame of the driving term F_d, until the libration damping (linewidth) reaches zero at the onset of self-sustained libration.

An implementation of a feedback loop that fulfills these conditions is shown in Fig. 1(b). Wherein, the output of a driven MEMS resonator is measured using a laser Doppler vibrometer (LDV), which measures the velocity. The LDV signal is down-converted using a lock-in amplifier, thus capturing the rotating frame dynamics, and passed through a band-pass filter so as to remove the dc component, which corresponds to the carrier frequency component. The upper cutoff frequency of the filter acts to limit the bandwidth of the feedback loop to within a desired range around the carrier. This output is then amplified, phase shifted, and used to modulate the carrier frequency, thus implementing a gain loop within the rotating frame of the driving force, which at the same time does not change the driven response due to that force (see Appendix A for more details on the experimental setup).

The dynamics of the librator are obtained by analyzing the system, including the feedback loop, using the RFA [24], where the displacement x is supposed to take the form $x(t) = R(t)\cos[\omega_d t + \phi(t)]$ with $R(t)$ and $\phi(t)$ the slowly varying amplitude and phase envelopes (slow flow variables). We introduce the complex phase space envelop $A(t) = Re^{i\phi}$ and its complex conjugate A^*. In addition, since the motion within the rotating frame consists of a steady-state amplitude component and a superimposed libration component, the slow-flow variables are further decomposed into $A(t) = A_0 + A_L(t)$, where $A_0 = R_0 e^{i\phi_0}$ is the static component, whereas $A_L(t) = R_L e^{i\phi_L}$ is the time-dependent libration component.

For low amplitude librations, the libration motion is considered to be centered around the steady-state component (A_0) that is obtained by solving the standard forced nonlinear resonator equation [24]. The dynamics are obtained by developing an expression for the feedback such that $f(t) = f[A(t), A(t)^*]$, which upon substitution into Eq. (1) and expansion we obtain the governing equations (see Appendix B for the detailed derivation)

$$
\begin{aligned}
\dot{A}_L &= -\left(i\delta_L + \tfrac{1}{2}\gamma_L\right)A_L + \tfrac{1}{8}(i3\alpha - \beta)h(A_L) + C_L A_L^*, \\
\dot{A}_L^* &= \left(i\delta_L - \tfrac{1}{2}\gamma_L\right)A_L^* - \tfrac{1}{8}(i3\alpha + \beta)h(A_L)^* + C_L^* A_L,
\end{aligned} \quad (2)
$$

with

$$
\gamma_L = \gamma + \tfrac{1}{2}\beta R_0^2 - \tfrac{1}{4}g\cos\theta, \tag{3a}
$$

$$
\delta_L = \delta - \tfrac{3}{4}\alpha R_0^2 + \tfrac{1}{8}g\sin\theta, \tag{3b}
$$

$$
h(A_L) = 2A_0 R_L^2 + A_0^* A_L^2 + R_L^2 A_L, \tag{3c}
$$

$$
C_L = \tfrac{1}{8}[(i3\alpha - \beta)A_0^2 - ge^{i\theta}], \tag{3d}
$$

where g is the loop gain, θ is the feedback phase, and δ_L and γ_L are respectively the effective detuning and effective linear damping of the libration motion A_L. The quadratic and cubic terms in A_L and A_L^* are collected in the functions $h(A_L)$ and $h(A_L)^*$, respectively.

Equations (2) form a two-dimensional autonomous system, which indicates that as long as the RFA is valid and higher-order terms can be safely neglected, the system cannot exhibit chaotic dynamics. Note that Eqs. (2) always have $A_L = A_L^* = 0$ as a fixed point, although not necessarily a stable one.

As the feedback gain term g is increased, the effective libration linewidth γ_L decreases until reaching zero for $g\cos\theta = 4\gamma + 2\beta R_0^2$, at which point a libration limit cycle is generated via a Hopf bifurcation. Near the Hopf bifurcation a libration frequency (ω_L) can be obtained by linearizing Eqs. (2), i.e., dropping the $h(A_L)$ and $h(A_L)^*$ terms, and calculating the eigenvalues of the system, which

gives

$$
\omega_L = \pm\mathrm{Re}\left[\sqrt{\delta_L^2 - |C_L|^2}\right]. \tag{4}
$$

Equation (4) gives the libration frequency ω_L for low amplitude librator limit cycles, i.e., $R_L \approx 0$. If we set $\gamma = \beta = g = 0$ then Eq. (4) reduces to the libration frequency of a Hamiltonian system, as given in Refs. [28,53].

III. EXPERIMENT AND DISCUSSION

Experimental investigation of librator dynamics are conducted using a piezoelectrically actuated GaAs heterostructure MEMS clamped-clamped beam device that is 100 μm in length, 20 μm wide, and 600 nm in thickness; see Refs. [17,54] for more information on the device fabrication. The device is placed in a vacuum chamber with a pressure of approximately 1 mPa, excited electrically, and its vibrations measured optically using a LDV. The actuation voltage, which is applied to both electrodes, generates piezoelectric stress in the mechanical resonator that leads to the bending of the resonator due to the built-in layered structure.

We measure and quantify the main device properties (see Appendix A and Refs. [17,47,55,56] for procedures of various parameter fittings) as follows: $\omega_0 = 2\pi \times 960$ kHz, a quality factor of 1042, and a scaled Duffing nonlinearity of $\alpha = 48$. We place the device in a feedback loop that is functionally equivalent to that shown in Fig. 1(b), and measure its response while the drive terms (F_d and ω_d) and the feedback gain (g) are swept (see Appendix A for details regarding the experimental setups). The experiments reported here are performed for $\theta = 0$.

A. Small amplitude libration

A first demonstration of a librator is performed for zero detuning, i.e., $\delta = 0$, and a drive voltage of 400 mV, placing the device well within the nonlinear regime, as shown in Fig. 2(a). The libration amplitude R_L is observed as the gain of the feedback loop is increased; see Fig. 2(b). When the loop gain crosses a critical threshold, γ_L becomes negative and the system exhibits a libration limit cycle generated via a Hopf bifurcation. The system is now a librator; see Figs. 2(c) to 2(e).

The sharp emergence of limit cycles near the threshold of self-oscillation is due to the facts that the intrinsic nonlinear damping is very small (approximately 5×10^{-3}) and that the limit cycle is stabilized by the saturation of the amplifier rather than the intrinsic nonlinear damping of the device. This is commonly the case in MEMS-based self-sustained oscillators [6,51]. However, as the limit cycle amplitude increases beyond the onset threshold, the scaling more closely resembles the well-known square root
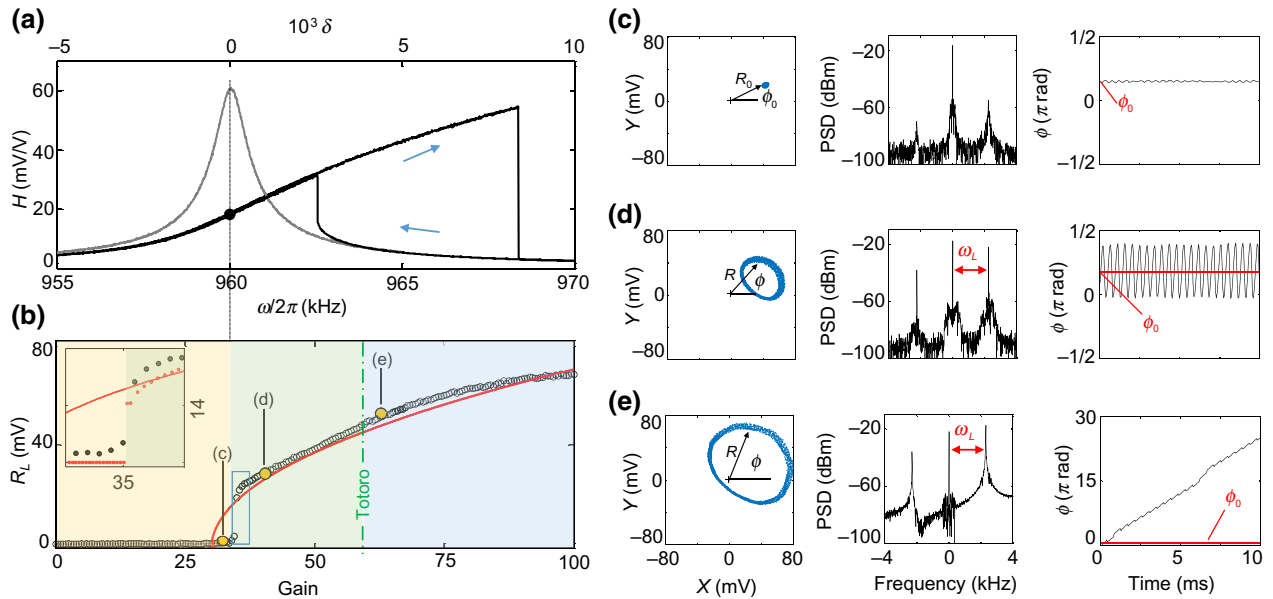
FIG. 2. (a) Measured spectral responses of the MEMS device for the linear ($F_d = 20$ mV) and nonlinear bistable ($F_d = 400$ mV) regimes, given in gray and black, respectively, and $\theta = 0$ for both. Here H denotes the relative amplitude response, expressed in millivolts measured per V drive. The blue arrows show the sweep direction for the lower and upper branches, and the vertical line at $\delta = 0$ indicates the parameters around which the librator is created. (b) Onset and amplitude of libration limit cycles as the feedback loop gain is increased. Different background colors indicate different operating regimes: before the Hopf bifurcation (yellow), after the Hopf bifurcation and before the totoro transition (green), and post totoro transition (blue). Experimental data points are shown as black circles, and a square root dependence is plotted to show the onset of the supercritical Hopf bifurcation around a gain of 33 (solid red line). The totoro transition is highlighted. The inset shows an enlarged view of the blue rectangle, where the experimental data (black dots) and Eq. (2)-based simulations (red dots) both show the onset of the limit cycle. The red trace in the inset is the same square root relation shown in the main plot. Details of subthreshold (c), librator (d), and rotator (e) operations. Panels show the rotating frame trajectories (left) as the gain is increased: first a limit cycle is created around the initial fixed point [(d), the system is a librator] then the orbit encompasses the phase space origin [(e), the system is a rotator]. The spectral response (middle panels) demonstrates the asymmetric nature of the librator; also clearly visible is the sideband overtaking the center frequency component as the system crosses the totoro transition. The libration frequency ω_L is indicated in red in the spectral responses. The phase (right panels), as extracted from the phase space trajectories, shows the steady-state phase ϕ_0 for subthreshold operation (c), the oscillating phase component with an average phase of ϕ_0 for the librator (d), and the unbounded phase for the rotator case (e). In all three cases the steady-state average phase is indicated (red).

relation; the libration amplitude versus gain data can be fitted to give a scaled effective nonlinear damping term of $\beta = 2.62$, as shown along with the numerical simulations in Fig. 2(b) [57].

Furthermore, Figs. 2(d) and 2(e) show an interesting transition as the limit cycle grows to encompass the origin of the rotating frame phase space. The rotations around the origin of the phase space plane determine the phase in the laboratory frame, i.e., the mean device frequency. If the librator limit cycle does not encompass the origin then the average phase of the system as seen in the laboratory frame is unchanged, i.e., $\langle \phi \rangle = \phi_0$ [Fig. 2(d)]. However, when the limit cycle does encompass the origin, the phase of the system starts to rotate, i.e., $\langle \phi \rangle \neq \phi_0$, and this free running phase changes the mean frequency of the system, i.e., the mean frequency is no longer that of the drive (ω_d), as shown in Fig. 2(e). This effect is further confirmed by observing that the magnitude of the libration

spectral peak(s) becomes larger than the magnitude of the driven central peak, as shown in the spectral responses in Figs. 2(c)–2(e).

Strictly speaking, this transition is simply a change in the mean frequency of the system and is not a bifurcation, since in two-dimensional phase space bifurcations require a creation or annihilation of fixed points or change of stability [8], which is not the case for this transition. Similar transitions have been identified, although not labeled, in the context of strongly forced oscillators [9,23,58,59], and more recently in the Kuramoto model [60]. In other contexts the case of zero average phase ($\langle \phi \rangle = \phi_0$) is referred to as libration, while the case of a free running phase ($\langle \phi \rangle \neq \phi_0$) is referred to as rotation [8,37]. Note that this nomenclature is not prevalent [38–41,61], but will be used here to distinguish the two regimes. Furthermore, throughout the text we identify this librator-to-rotator transition by the acronym "totoro."
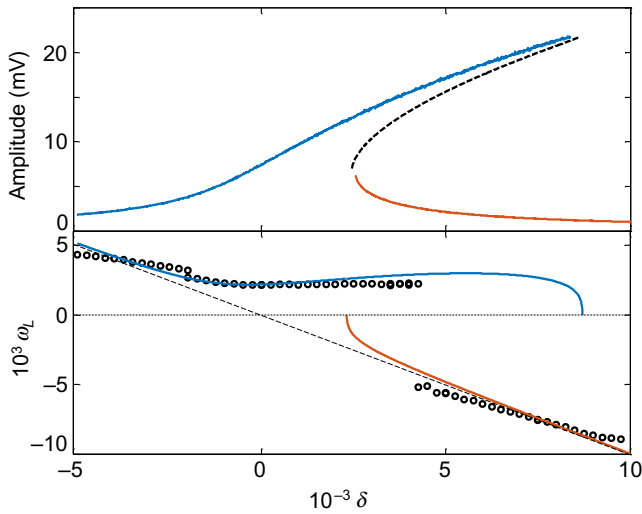
FIG. 3. Dependence of the libration frequency on detuning. The nonlinear Duffing response (top panel) is shown as a visual reference. We represent the upper and lower measured branches by blue and red traces, respectively, and the unstable branch (calculated) by the dashed black line. The measured libration frequency at the onset of the Hopf bifurcation (bottom panels). The measured values are shown with black circles, and the solid lines correspond to the analytically calculated libration frequencies, as given by Eq. (4), for the upper (blue) and lower (red) branches. Note that, for large detunings, the libration frequency practically follows the linear relation $\omega_{\text{Libration}} = -\delta$, shown as the black dashed line. The areas with no experimental data correspond to parameters where the system is not stable enough to perform the measurements.

Subsequently, we sweep the drive frequency ω_d while maintaining a constant driving force of $F_d = 400$ mV, and determine the librator's frequency around the onset of the Hopf bifurcation for each of the drive frequencies. This collection of ω_L is plotted as a function of the detuning parameter δ, as shown in Fig. 3 along with values calculated from Eq. (4).

Particularly interesting is the bistable interval. Since two possible steady-state solutions exist, then there equally exist the possibility to induce two libration limit cycles around each one of those solutions, although not simultaneously. As can be seen in Fig. 3, the libration frequency drops to zero around the saddle-node bifurcations, where one of the stable fixed points and the saddle point collide. Whether within or outside the bistable region, the small amplitude librator frequency agrees relatively well with the analytical calculations, further confirming the linearization in Eq. (4), whereas the discrepancy between data and model in Fig. 3 is due to frequency drift over long duration measurements.

B. Large amplitude behavior

The possibility to generate two types of limit cycles centered around each of the steady-state solution branches

merits an in-depth look at the large amplitude response of the librator. For one, libration limit cycles around the low-amplitude branch (LB) and the high-amplitude branch (HB) orbit their respective fixed points in opposite directions, clockwise and counterclockwise, respectively, as can be seen from the experimental data in Fig. 4(a). This indicates that the LB librator has a dominant negative frequency component within the rotating frame, while the HB librator has a dominant positive frequency component within the rotating frame. Indeed, previous work has found that driven or even stochastic librations tend to show a strong asymmetry depending on detuning [27,28,53].

At larger amplitudes, both the HB and LB limit cycles are bounded by homoclinic bifurcations, i.e., limit cycles with infinitely long periods that pass through the saddle point. As the gain of the feedback loop is increased, the limit cycles approach the homoclinics and, as a consequence, their frequency reduces as their amplitude increases. Thus, librators exhibit a very strong nonlinearity whereby their frequency starts with ω_L as given by Eq. (4) for $A_L \approx 0$, and ends with $\omega_L = 0$ for $A_L = A_{\text{Homoclinic}}$. Experimental and numerical demonstrations of this slowing down near the homoclinics are shown in Fig. 4(b), where the libration (or rotation) frequency is plotted as a function of the distance between a limit cycle trajectory and the respective homoclinic trajectory [$A_{\text{Homoclinic}} - \max(R_L)$].

As the gain is increased beyond the homoclinic bifurcations, the limit cycles, whether originally orbiting the HB or LB, transition to a new regime, one whose orbit now encompasses all three fixed points and rotates in a counterclockwise fashion; see Fig. 4(a). This additional limit cycle is made possible by the fact that the three fixed points have a cumulative index number of 1, and would not have been possible in a two-dimensional phase space exhibiting only two fixed points [62]. These wide limit cycles are in fact always rotators, whereas prior to the homoclinic bifurcation the limit cycles can be either librators or rotators. Furthermore, they demonstrate the same scaling behavior as their progenitor limit cycles, i.e., slowing down as they approach the homoclinic, as shown in Fig. 4(b). Here too some discrepancy is visible between the experimental and analytical data; as before, this is due to frequency drift but is further compounded by the coarse fitting of the nonlinear damping term.

The transition between the different limit cycle regimes underlines limitations in the librator model. For one, it is important to keep in mind that the librator dynamics, whether small or large amplitude, are defined around a dc component. Therefore, if the system is in some condition that destabilizes the steady state, i.e., a transition from the high branch to the low branch, then the transient is not accounted for by the current model. Furthermore, the librator, as implemented by the feedback loop shown in Fig. 1(b), revolves around a dc component that we have
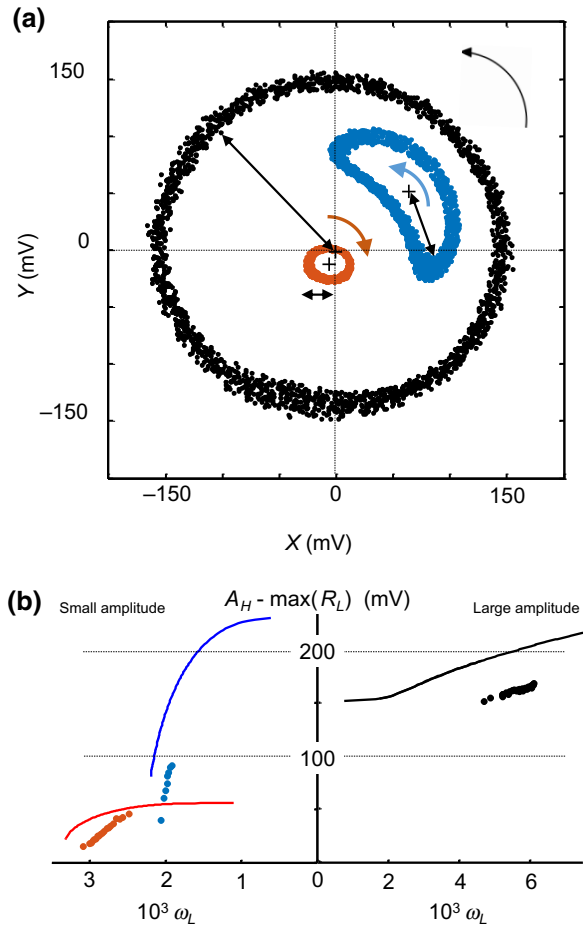
(a)

(b)

FIG. 4. (a) Libration and rotation orbits obtained for $F_d = 0.6$ V. Orbiting counterclockwise for the high amplitude branch (blue) and the large rotator regime (black), and clockwise around the low amplitude branch (red). The black double-sided arrows indicate the maximum libration distance with respect to the fixed points (in the case of the large amplitude rotation it is with respect to the origin). The black and blues traces are obtained for $\delta = 2.6 \times 10^{-3}$ (but for different amplifier settings), while the red trajectory is obtained for $\delta = 3.6 \times 10^{-3}$. (b) Scaling of libration or rotation frequency as a function of the distance between the homoclinic and the maximum libration distance $[A_{\text{Homoclinic}} - \max(R_L)]$. The left panel represents the libration or rotation frequency prior to the crossing of the homoclinic bifurcation, with the high-branch and low-branch data shown in blue and red, respectively (circles represent experimental data and solid lines represent simulation data). The right panel shows the scaling post the homoclinic bifurcation. The mismatch between the simulation and measurements indicates experimental frequency drift and amplitude calibration drift.

approximated by the steady-state solution(s) to the driven Duffing equation. When the librator transitions to the large rotation orbits, such an approximation is no longer valid as the difference between the dc component (the mean value of A_L over an orbit) and the steady-state solution is significant. Indeed, for the large rotation orbits, we rewrite

the dynamics equation as one that is independent of the steady-state solutions, which reads (see Appendix B for a detailed derivation)

$$i\dot{A}_L - \delta A_L + \frac{i\gamma}{2}A_L + \frac{3\alpha}{8}|A_L|^2 A_L + \frac{i\beta}{8}|A_L|^2 A_L$$
$$= \frac{1}{2}\left(F_d + \frac{ig}{4}(A_L e^{-i\theta} - A_L^* e^{i\theta})\right). \quad (5)$$

The piecewise model is a consequence of this limitation, where Eqs. (2) are used for libration around the fixed points (with the respective parameters accounted for) and Eq. (5) is used for the large amplitude orbits.

On a side note, the combined presence of a harmonic drive and a limit cycle may be confused with the case of a forced oscillator; however, the two represent largely distinct dynamics and bifurcation diagrams. The fundamental difference between the two being that in the case of the librator the driving force creates a certain phase space topology that is largely unchanged by the limit cycle, whereas in the case of a forced oscillator, the limit cycle and the driving force interact to create the topology. As a consequence, the two systems exhibit widely differing behavior. For one, a forced oscillator locks its frequency and phase in response to weak external forcing, whereas the librator, virtually by definition, does not. If the external forcing is highly detuned, a forced oscillator can experience desynchronization, leading to phase slips via a SNIC (saddle node on an invariant circle) bifurcation, whereas the librator only changes its frequency as the detuning is changed. Furthermore, under the effect of strong external forcing, nonisochronous oscillators exhibit highly complicated bifurcation diagrams [9,58,59,63] with the potential to generate chaos [64–66], whereas the librator, as stated, does not produce a steady-state chaotic output. Incidentally, one feature that is common to both forced oscillators and librators is the possibility to observe totoro transitions, since it can be argued that such transitions are common to multifrequency dynamical systems [23,60].
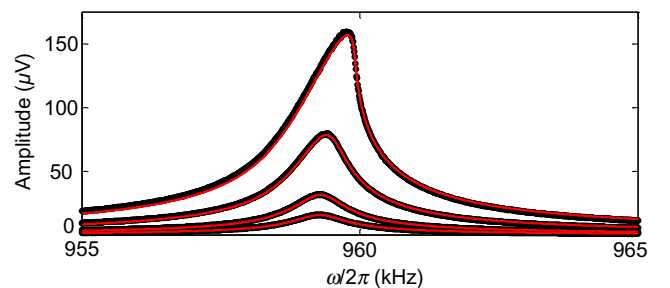

FIG. 5. Fits of the nonlinear resonance response. A few examples of the experimental nonlinear responses (black circles) and their fits (red lines) for drive amplitudes of 20, 50, 100, and 150 mV for the curves with increasing amplitudes, respectively.

IV. CONCLUSIONS

Several exciting prospects for further investigation of librators are possible. For one, the use of nonlinear resonators with higher-order nonlinearity, say quintic nonlinearity [67–69], implies the possibility of even more distinct limit cycles and homoclinic bifurcations within the same phase space, which is an outlook of practical and fundamental interest [70–72]. Indeed, even in the system presented in this work rigorous accounts of the existence and number of limit cycles (both stable and unstable) were not fully given, and these issues remain to be addressed on a theoretical and numerical level.

Furthermore, that a librator may be synchronized by the application of weak external forcing, in a manner similar to the way oscillators can be synchronized, is worth investigating. Furthermore, the formation of a librator network, potentially within a single multimode device [18], could be of great practical importance.

On an experimental note, it may be possible to produce a feedback loop-free librator, in which thermomechanical back action can theoretically trigger a Hopf bifurcation in a driven high quality factor nanomechanical resonator [73], although this remains to be proven experimentally. On the other hand, if one accepts that $F_d \gg f$ (below the totoro transition) then the lock-in amplifier can be replaced with an envelope detector, thus greatly simplifying the experimental setup.

In summary, this work introduced the "librator" as an alternative dynamical mode of operating nonlinear MEMS devices, in which a quasiperiodic output is generated through the creation of limit cycles within the rotating frame of a driven nonlinear MEMS resonator. These limit cycles do not change the global topology of the rotating frame that is created by the driving force, but are rather constrained by it. Different types of limit cycles are observed, along with homoclinic bifurcations. These bifurcations do not induce chaos as the system is contained within a two-dimensional phase space. Interestingly, the dynamics presented here can be applied to other physical implementations of weakly nonlinear and weakly damped resonators, such as optical and superconducting ones.

ACKNOWLEDGMENTS

APPENDIX A: EXPERIMENTAL SETUPS AND PROCEDURES

The Duffing parameter is characterized using a series of nonlinear frequency response curves, which are obtained using a Zurich Instruments lock-in amplifier (HF2LI) under a $-0.5\ V_{dc}$ bias. The negative bias is applied to avoid electrical nonlinearities in the metal-semiconductor
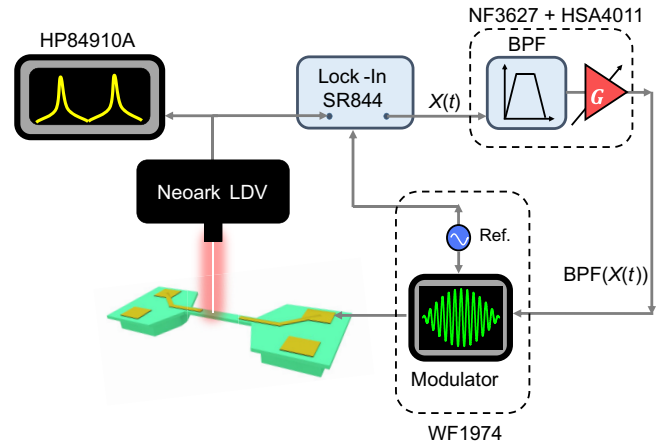

FIG. 6. Schematic representation of the implementation of the librator feedback loop.

contact [54]. The fits, some of which are shown in Fig. 5, follow the procedure detailed in Refs. [17,55].

Throughout the measurement period, a very slow (day time scale) frequency drift is observed in the device; this is accounted for by performing a spectral response sweep before each measurement run. This slow frequency drift only affects ω_0 and δ, but has no impact on the quality factor and the nonlinear terms. We implement the feedback loop as shown in Fig. 6 using the following instruments: a Neoark LDV (Neoark Corporation) with a 100 MHz bandwidth and a 10 (m/s)/v sensitivity is used to measure the device; a lock-in amplifier (SR844, SRS) to downconvert the output from the LDV, and subsequently a filter-amplifier (NF37627, NF corporation) to filter and amplify the X quadrature from the output of the lock-in; a vector signal analyzer (VSA, HP89410A, Keysight) equally samples the output of the LDV. We use the output from the filter-amplifier to perform a double-sideband transmitted carrier amplitude modulation (DSB TC AM) using a waveform generator (WF1974, NF corporation). Because the modulation depth is limited to 100%, this imposes a limit on the feedback amplitude such that $|f| = F_d$.

To obtain Fig. 4, a double-sideband suppressed carrier (DSB SC) is used, with an additional drive tone generated using an independent channel on the signal generator, which we do to overcome the modulation depth limitation of the DSB-TC configuration. Furthermore, the nature of the used electronic filter is such that a high feedback loop gain can potentially ring the filter itself, i.e., turn the filter into an oscillator. The output from the system is closely monitored during measurements, to ensure that such behavior does not occur.

APPENDIX B: DERIVATION OF LIBRATOR DYNAMICS

We start by deriving a closed form for the term f in Eq. (1). Using the RFA, i.e., $x(t) = \frac{1}{2}(Ae^{i\omega t} + A^* e^{-i\omega t})$, the

output of the LDV is then given as

$$\dot{x}(t) = \frac{i\omega}{2}(Ae^{i\omega t} - A^*e^{-i\omega t}) + \frac{1}{2}(\dot{A}e^{i\omega t} + \dot{A}^*e^{-i\omega t}). \quad \text{(B1)}$$

After multiplying the LDV output with the reference tone, i.e., $\cos(\omega t)$, we obtain

$$
\begin{aligned}
S(t) &= \dot{x}(t)\cos(\omega t + \theta) \\
&= \frac{i\omega}{4}(Ae^{i(2\omega t+\theta)} + Ae^{-i\theta} - A^*e^{i\theta} - A^*e^{-i(2\omega t+\theta)}) \\
&\quad + \frac{1}{4}(\dot{A}e^{i(2\omega t+\theta)} + \dot{A}e^{-i\theta} + \dot{A}^*e^{i\theta} + \dot{A}^*e^{-i(2\omega t+\theta)}),
\end{aligned}
$$
$$\text{(B2)}$$

where θ is an arbitrary phase difference. After removing the high-frequency components, as a result of the band-pass filter (BPF), Eq. (B2) reduces to

$$S(t) = \frac{i\omega}{4}(Ae^{-i\theta} - A^*e^{i\theta}) + \frac{1}{4}(\dot{A}e^{-i\theta} + \dot{A}^*e^{i\theta}). \quad \text{(B3)}$$

We consider that $\omega A \gg \dot{A}$, and thus drop the second term from the above equation, giving

$$S(t) \approx \frac{i\omega}{4}(Ae^{-i\theta} - A^*e^{i\theta}). \quad \text{(B4)}$$

Since we decomposed the complex amplitude into a steady-state dc component and a libration ac component, i.e., $A(t) = A_{\text{dc}} + A_{\text{ac}}(t) = A_0 + A_L(t)$, the BPF also removes the dc component from the signal, thus reducing $S(t)$ to

$$\omega S_{\text{ac}}(t) = \frac{i\omega}{4}(A_L e^{-i\theta} - A_L^* e^{i\theta}). \quad \text{(B5)}$$

The signal is then amplified by a factor g and possibly phase shifted to give $f = gS_{\text{ac}}$. We consider that any additional phase shift can still be contained within the θ term, to give

$$f = g\omega S_{\text{ac}}(t) = \frac{ig\omega}{4}(A_L e^{-i\theta} - A_L^* e^{i\theta}). \quad \text{(B6)}$$

We rewrite Eq. (1) as

$$
\begin{aligned}
\ddot{x} + (\gamma + \beta x^2)\dot{x} + \omega_0^2 x + \alpha x^3 \\
= [F_d + g\omega S_{\text{ac}}(t)]\cos(\omega_d t). \quad \text{(B7)}
\end{aligned}
$$

We apply the standard RFA approximations to Eq. (B7), where we introduce $x(t) = \frac{1}{2}(Ae^{i\omega t} + A^*e^{-i\omega t})$ into Eq.

(B7) and keep only the $\omega_d t$ terms of first order to give

$$\ddot{x} \approx \frac{-\omega_d^2}{2}Ae^{i\omega_d t} + \frac{i\omega}{2}\dot{A}e^{i\omega_d t},$$

$$\gamma\dot{x} \approx \frac{i\omega_d\gamma}{2}Ae^{i\omega_d t},$$

$$\alpha x^3 \approx \frac{3\alpha}{8}AA^*Ae^{i\omega_d t},$$

$$\beta x^2\dot{x} \approx \frac{i\beta}{8}AA^*Ae^{i\omega_d t},$$

$$\omega_0^2 x \approx \frac{\omega_0^2}{2}Ae^{i\omega_d t},$$

$$\omega_d^2 \approx \omega_0^2(1 + 2\delta).$$

Thus, Eq. (B7) becomes (in nondimensional form)

$$
\begin{aligned}
i\dot{A} - \delta A + \frac{i\gamma}{2}A + \frac{3\alpha}{8}AA^*A + \frac{i\beta}{8}AA^*A \\
= \frac{1}{2}[F_d + gS_{\text{ac}}(t)]. \quad \text{(B8)}
\end{aligned}
$$

If the libration motion is centered around one of the two branches then we approximate the dc component to the steady-state solution of a forced Duffing, we split the complex amplitude into the two equations

$$\left(-\delta + \frac{3\alpha}{8}|A_0|^2\right)A_0 + i\left(\frac{\gamma}{2} + \frac{\beta}{8}|A_0|^2\right)A_0 = \frac{F_d}{2} \quad \text{(B9)}$$

and

$$
\begin{aligned}
i\dot{A}_L &- \delta A_L + \frac{i\gamma}{2}A_L \\
&+ \frac{3\alpha}{8}(2|A_0|^2 A_L + A_0^2 A_L^* + 2|A_L|^2 A_0 + A_0^* A_L^2 + |A_L|^2 A_L) \\
&+ \frac{i\beta}{8}(2|A_0|^2 A_L + A_0^2 A_L^* + 2|A_L|^2 A_0 + A_0^* A_L^2 + |A_L|^2 A_L) \\
&= \frac{ig}{8}(A_L e^{-i\theta} - A_L^* e^{i\theta}). \quad \text{(B10)}
\end{aligned}
$$

Equation (B9) is the standard RFA of a driven Duffing, while by rearranging Eq. (B10) we obtain Eqs. (2) from the main text.

If, on the other hand, the libration is in the regime of the large amplitude limit cycle where the orbit encircles all three fixed points then, due to the almost circular shape of the orbit and the fact that it is nearly centered around the origin of the phase space, we approximate the dc

component to zero, i.e., $A_{dc} \approx 0$; thus, Eq. (B8) becomes

$$i\dot{A}_L - \delta A_L + \frac{i\gamma}{2}A_L + \frac{3\alpha}{8}|A_L|^2 A_L + \frac{i\beta}{8}|A_L|^2 A_L$$
$$= \frac{1}{2}\left(F_d + \frac{ig}{4}(A_L e^{-i\theta} - A_L^* e^{i\theta})\right). \qquad \text{(B11)}$$

[1] Alejandro Jenkins, Self-oscillation, Phys. Rep. **525,** 167 (2013).

[2] Alfred Brian Pippard, *The Physics of Vibration* (Cambridge University Press, Cambridge, 2007).

[3] Leon Glass, Synchronization and rhythmic processes in physiology, Nature **410,** 277 (2001).

[4] Leon Glass and Michael C. Mackey, *From Clocks to Chaos* (Princeton University Press, Princeton, 2020).

[5] Balth Van Der Pol, Vii. forced oscillations in a circuit with non-linear resistance.(reception with reactive triode), London, Edinburgh, Dublin Philos. Mag. J. Sci. **3,** 65 (1927).

[6] Eric Vittoz, *Low-Power Crystal and MEMS Oscillators: the Experience of Watch Developments* (Springer Science & Business Media, Berlin, 2010).

[7] J. T. M. Van Beek and Rob Puers, A review of mems oscillators for frequency reference and timing applications, J. Micromech. Microeng. **22,** 013001 (2011).

[8] Steven H. Strogatz, *Nonlinear Dynamics and Chaos with Student Solutions Manual: With Applications to Physics, Biology, Chemistry, and Engineering* (CRC press, Boca Raton, 2018).

[9] Arkady Pikovsky, Jurgen Kurths, Michael Rosenblum, and Jürgen Kurths, *Synchronization: a Universal Concept in Nonlinear Sciences* (Cambridge university press, 2003), Vol. 12.

[10] Daniel M. Abrams and Steven H. Strogatz, Chimera States for Coupled Oscillators, Phys. Rev. Lett. **93,** 174102 (2004).

[11] Y. Kuramoto, *Chemical Oscillations, Waves, and Turbulence* (Springer-Verlag, Berlin, 1984).

[12] Jacob Torrejon, Mathieu Riou, Flavio Abreu Araujo, Sumito Tsunegi, Guru Khalsa, Damien Querlioz, Paolo Bortolotti, Vincent Cros, Kay Yakushiji, and Akio Fukushima *et al.*, Neuromorphic computing with nanoscale spintronic oscillators, Nature **547,** 428 (2017).

[13] Gouhei Tanaka, Toshiyuki Yamane, Jean Benoit Héroux, Ryosho Nakane, Naoki Kanazawa, Seiji Takeda, Hidetoshi Numata, Daiju Nakano, and Akira Hirose, Recent advances in physical reservoir computing: A review, Neural Netw. **115,** 100 (2019).

[14] S. Houri, S. J. Cartamil-Bueno, M. Poot, P. G. Steeneken, H. S. J. van der Zant, and W. J. Venstra, Direct and parametric synchronization of a graphene self-oscillator, Appl. Phys. Lett. **110,** 073103 (2017).

[15] Thomas Barois, S. Perisanu, Pascal Vincent, Stephen T. Purcell, and Anthony Ayari, Frequency modulated self-oscillation and phase inertia in a synchronized nanowire mechanical resonator, New J. Phys. **16,** 083009 (2014).

[16] Damián H. Zanette, Stability of two-mode internal resonance in a nonlinear oscillator, Eur. Phys. J. B **91,** 1 (2018).

[17] S. Houri, D. Hatanaka, M. Asano, R. Ohta, and H. Yamaguchi, Limit cycles and bifurcations in a nonlinear mems resonator with a 1: 3 internal resonance, Appl. Phys. Lett. **114,** 103103 (2019).

[18] S. Houri, D. Hatanaka, M. Asano, and H. Yamaguchi, Demonstration of Multiple Internal Resonances in a Microelectromechanical Self-Sustained Oscillator, Phys. Rev. Appl. **13,** 014049 (2020).

[19] Johannes Güttinger, Adrien Noury, Peter Weber, Axel Martin Eriksson, Camille Lagoin, Joel Moser, Christopher Eichler, Andreas Wallraff, Andreas Isacsson, and Adrian Bachtold, Energy-dependent path of dissipation in nanomechanical resonators, Nat. Nanotechnol. **12,** 631 (2017).

[20] I. Mahboob, R. Dupuy, K. Nishiguchi, A. Fujiwara, and H. Yamaguchi, Hopf and period-doubling bifurcations in an electromechanical resonator, Appl. Phys. Lett. **109,** 073101 (2016).

[21] David A. Czaplewski, Scott Strachan, Oriel Shoshani, Steven W. Shaw, and Daniel López, Bifurcation diagram and dynamic response of a mems resonator with a 1: 3 internal resonance, Appl. Phys. Lett. **114,** 254104 (2019).

[22] C. Van der Avoort, R. Van der Hout, J. J. M. Bontemps, P. G. Steeneken, K. Le Phan, R. H. B. Fey, J. Hulshof, and J. T. M. Van Beek, Amplitude saturation of mems resonators explained by autoparametric resonance, J. Micromech. Microeng. **20,** 105012 (2010).

[23] Arkady Pikovsky, Michael Rosenblum, and Jürgen Kurths, Phase synchronization in regular and chaotic systems, Int. J. Bifurcat. Chaos **10,** 2291 (2000).

[24] Andrew N. Cleland, *Foundations of Nanomechanics: from Solid-State Theory to Device Applications* (Springer Science & Business Media, Heidelberg, 2013).

[25] Silvan Schmid, Luis Guillermo Villanueva, and Michael Lee Roukes, *Fundamentals of nanomechanical resonators*, Vol. 49 (Springer).

[26] Mohammad I. Younis, *MEMS Linear and Nonlinear Statics and Dynamics* (Springer Science & Business Media, New York, 2011), Vol. 20.

[27] Jana S. Huber, Gianluca Rastelli, Maximilian J Seitner, Johannes Kölbl, Wolfgang Belzig, Mark I. Dykman, and Eva M. Weig, Spectral Evidence of Squeezing of a Weakly Damped Driven Nanomechanical Mode, Phys. Rev. X **10,** 021066 (2020).

[28] Samer Houri, Motoki Asano, Hiroshi Yamaguchi, Natsue Yoshimura, Yasuharu Koike, and Ludovico Minati, Generic Rotating-Frame-Based Approach to Chaos Generation in Nonlinear Micro-And Nanoelectromechanical System Resonators, Phys. Rev. Lett. **125,** 174301 (2020).

[29] Hiroshi Yamaguchi and Samer Houri, Generation and Propagation of Topological Solitons in a Chain of Coupled Parametric-Micromechanical-Resonator Arrays, Phys. Rev. Appl. **15,** 034091 (2021).

[30] Motoki Asano, Ryuichi Ohta, Takuma Aihara, Tai Tsuchizawa, Hajime Okamoto, and Hiroshi Yamguchi, Optically probing schwinger angular momenta in a

micromechanical resonator, Phys. Rev. A **100**, 053801 (2019).

[31] Balth Van der Pol, Lxxxviii. on "relaxation-oscillations", London, Edinburgh, Dublin Philos. Mag. J. Sci. **2**, 978 (1926).

[32] Satadal Datta, Bifurcations of a van der pol oscillator in a double well, arXiv:1709.10126 (2017).

[33] Hussam Alhussein and Mohammad F. Daqaq, Potential well escape in a galloping twin-well oscillator, Nonlinear Dynam. **99**, 57 (2020).

[34] Giovanni Domenico Cassini, *De l'origine et du Progrés de l'Astronomie, et de son Usage Dans la Geographie et Dans la Navigation* (De l'Imprimerie Royale, Paris, 1730).

[35] R. W. Farquhar, *The Control and Use of Libration-Point Satellites* (Stanford University, Stanford, 1969).

[36] Kathleen C. Howell, Brian T. Barden, and Martin W. Lo, Application of dynamical systems theory to trajectory design for a libration point mission, J. Astronaut. Sci. **45**, 161 (1997).

[37] N. V. Alexeeva, I. V. Barashenkov, and G. P. Tsironis, Impurity-Induced Stabilization of Solitons in Arrays of Parametrically Driven Nonlinear Oscillators, Phys. Rev. Lett. **84**, 3053 (2000).

[38] Florian Lenz, Fotis K. Diakonos, and Peter Schmelcher, Classical dynamics of the time-dependent elliptical billiard, Phys. Rev. E **76**, 066213 (2007).

[39] Yoshiki Nakajima and Shigeo Naya, Orientational phase transition and dynamic susceptibility of hindered-rotating dipolar system–a librator-rotator model–, J. Phys. Soc. Jpn. **63**, 904 (1994).

[40] J. M. Rost, J. C. Griffin, B. Friedrich, and D. R. Herschbach, Pendular States and Spectra of Oriented Linear Molecules, Phys. Rev. Lett. **68**, 1299 (1992).

[41] Bretislav Friedrich and Dudley Herschbach, Alignment and Trapping of Molecules in Intense Laser Fields, Phys. Rev. Lett. **74**, 4623 (1995).

[42] Mahmood Bagheri, Menno Poot, Mo Li, Wolfram P. H. Pernice, and Hong X. Tang, Dynamic manipulation of nanomechanical resonators in the high-amplitude regime and non-volatile mechanical memory operation, Nat. Nanotechnol. **6**, 726 (2011).

[43] Samer Houri, Ryuichi Ohta, Motoki Asano, Yaroslav M. Blanter, and Hiroshi Yamaguchi, Pulse-width modulated oscillations in a nonlinear resonator under two-tone driving as a means for mems sensor readout, Jpn. J. Appl. Phys. **58**, SBBI05 (2019).

[44] David A. Czaplewski, Changyao Chen, Daniel Lopez, Oriel Shoshani, Axel M. Eriksson, Scott Strachan, and Steven W. Shaw, Bifurcation Generated Mechanical Frequency Comb, Phys. Rev. Lett. **121**, 244302 (2018).

[45] Avishek Chowdhury, Marcel G. Clerc, Sylvain Barbay, Isabelle Robert-Philip, and Remy Braive, Weak signal enhancement by nonlinear resonance control in a forced nano-electromechanical resonator, Nat. Commun. **11**, 1 (2020).

[46] Thomas Antoni, Kevin Makles, Rémy Braive, Tristan Briant, Pierre-François Cohadon, Isabelle Sagnes, Isabelle Robert-Philip, and Antoine Heidmann, Nonlinear mechanics with suspended nanomembranes, EPL (Europhys. Lett.) **100**, 68005 (2013).

[47] Stav Zaitsev, Oleg Shtempluck, Eyal Buks, and Oded Gottlieb, Nonlinear damping in a micromechanical oscillator, Nonlinear Dynam. **67**, 859 (2012).

[48] B. Yurke, D. S. Greywall, A. N. Pargellis, and P. A. Busch, Theory of amplifier-noise evasion in an oscillator employing a nonlinear resonator, Phys. Rev. A **51**, 4211 (1995).

[49] R. van Leeuwen, D. M. Karabacak, H. S. J. van der Zant, and W. J. Venstra, Nonlinear dynamics of a microelectromechanical oscillator with delayed feedback, Phys. Rev. B **88**, 214301 (2013).

[50] L. G. Villanueva, E. Kenig, R. B. Karabalin, M. H. Matheny, Ron Lifshitz, M. C. Cross, and M. L. Roukes, Surpassing Fundamental Limits of Oscillators Using Nonlinear Resonators, Phys. Rev. Lett. **110**, 177208 (2013).

[51] Changyao Chen, Damián H. Zanette, Jeffrey R. Guest, David A. Czaplewski, and Daniel López, Self-Sustained Micromechanical Oscillator with Linear Feedback, Phys. Rev. Lett. **117**, 017203 (2016).

[52] Ryuichi Ohta, Hajime Okamoto, and Hiroshi Yamaguchi, Feedback control of multiple mechanical modes in coupled micromechanical resonators, Appl. Phys. Lett. **110**, 053106 (2017).

[53] J. S. Ochs, M Seitner, M. I. Dykman, and E. M. Weig, Amplification and spectral evidence of squeezing in the response of a strongly driven nanoresonator to a probe field, Phys. Rev. A **103**, 013506 (2021).

[54] Hiroshi Yamaguchi, Gaas-based micro/nanomechanical resonators, Semicond. Sci. Tech. **32**, 103003 (2017).

[55] Dejan Davidovikj, Farbod Alijani, Santiago J. Cartamil-Bueno, Herre S. J. van der Zant, Marco Amabili, and Peter G. Steeneken, Nonlinear dynamic characterization of two-dimensional materials, Nat. Commun. **8**, 1 (2017).

[56] Pavel M. Polunin, Yushi Yang, Mark I. Dykman, Thomas W. Kenny, and Steven W. Shaw, Characterization of mems resonator nonlinearities using the ringdown response, J. Microelectromech. S. **25**, 297 (2016).

[57] The shape and scale of the numerically obtained points (red dots) in the inset of Fig. 2(b) are accurate; however, the onset of self-oscillation obtained from simulation is centered around a gain value of $g = 32$, due to the coarse calibration of gain and nonlinear damping from the experimental data. For visual clarity, the numerical points are shifted to overlap with the experimental data.

[58] P. J. Holmes and D. A. Rand, Bifurcations of the forced van der pol oscillator, Q. Appl. Math. **35**, 495 (1978).

[59] G. V. Levina and A. A. Nepomnyaschiy, Analysis of an amplitude equation for autovibrational flow regimes at resonance external forces, J. Appl. Math. Mech.-USS **66**, 241 (1986).

[60] E. A. P. Wright, S. Yoon, J. F. F. Mendes, and A. V. Goltsev, Missed topological phase transition in the forced kuramoto model, arXiv:2012.08882 (2020).

[61] Ricardo Lima and Dima Shepelyansky, Fast Delocalization in a Model of Quantum Kicked Rotator, Phys. Rev. Lett. **67**, 1377 (1991).

[62] Floris Takens, Forced oscillations and bifurcations, Applications of Global Analysis I, Sympos., Utrecht State Univ., Utrecht, 1973, Commun. Math. Inst., Rijksuniv. Utrecht 3, 1–59 (1974 **3**, 1–62 (2001).

[63] Catalina Mayol, Raúl Toral, Claudio R. Mirasso, and Mario A. Natiello, Class-a lasers with injected signal: Bifurcation set and lyapunov–potential function, Phys. Rev. A **66,** 013808 (2002).

[64] Hitoshi Kawaguchi and Kenju Otsuka, A new class of instabilities in a diode laser with an external cavity, Appl. Phys. Lett. **45,** 934 (1984).

[65] Eok-Kyun Lee, Hyun-Soo Pang, Jong-Dae Park, and Hoyun Lee, Bistability and chaos in an injection-locked semiconductor laser, Phys. Rev. A **47,** 736 (1993).

[66] T. B. Simpson, J. M. Liu, A. Gavrielides, V. Kovanis, and P. M. Alsing, Period-doubling route to chaos in a semiconductor laser subject to optical injection, Appl. Phys. Lett. **64,** 3539 (1994).

[67] Najib Kacem, Sébastien Baguet, Laurent Duraffourg, Georges Jourdan, Régis Dufour, and Sébastien Hentz, Overcoming limitations of nanomechanical resonators with simultaneous resonances, Appl. Phys. Lett. **107,** 073105 (2015).

[68] Chandan Samanta, Nishta Arora, and A. K. Naik, Tuning of geometric nonlinearity in ultrathin nanoelectromechanical systems, Appl. Phys. Lett. **113,** 113101 (2018).

[69] Linhai Huang, S. M. Soskin, I. A. Khovanov, R. Mannella, K Ninios, and Ho Bun Chan, Frequency stabilization and noise-induced spectral narrowing in resonators with zero dispersion, Nat. Commun. **10,** 1 (2019).

[70] Vladimir Igorevich Arnol'd, Loss of stability of self-oscillations close to resonance and versal deformations of equivariant vector fields, Funct. Anal. Appl. **11,** 85 (1977).

[71] N. V. Kuznetsov, O. A. Kuznetsova, and G. A. Leonov, Visualization of four normal size limit cycles in two-dimensional polynomial quadratic system, Differ. Equ. Dyn. Syst. **21,** 29 (2013).

[72] Anina Leuch, Luca Papariello, Oded Zilberberg, Christian L. Degen, Ramasubramanian Chitra, and Alexander Eichler, Parametric Symmetry Breaking in a Nonlinear Resonator, Phys. Rev. Lett. **117,** 214101 (2016).

[73] Mark I. Dykman, Gianluca Rastelli, Michael L. Roukes, and Eva M. Weig, Resonantly Induced Friction and Frequency Combs in Driven Nanomechanical Systems, Phys. Rev. Lett. **122,** 254301 (2019).